Aggregation of Silica Nanoparticles in an Aqueous Suspension

Lande Liu
Dept. of Chemical Sciences, University of Huddersfield, Huddersfield HD1 3DH, UK

DOI 10.1002/aic.14839
Published online April 20, 2015 in Wiley Online Library (wileyonlinelibrary.com)

Aggregation affects the stability of the nanoparticles in fluids. For hydrophilic particles in aqueous suspensions, zeta potential becomes a common measure to control the stability of the particles. However, it is not clear how zeta potential impacts on the interaction of the particles during their close range contact when the hydration repulsion arises strongly. This article demonstrates a method that uses the kinetic theory of aggregation for an aggregation system of changing zeta potential to determine the hydration repulsion and the aggregation efficiency. It was found that the hydration repulsion has an equivalent electrical potential of 30 mV on the stem surface of the particles and an exponential decay length of 2.77 Å. This hydration potential is equivalent to 12 mV zeta potential and contributes 29% to the aggregation coefficient that is 5.5 × 10^{-6} for a 30 mV zeta potential stabilized silica particle suspension. © 2015 American Institute of Chemical Engineers *AIChE J*, 61: 2136–2146, 2015

Keywords: aggregation, collision success factor, hydration repulsion, nanoparticles, population balance

Introduction

Solid nanoparticles in fluids, also referred as nanosuspensions or nanofluids, have found a wide range of applications[1,2] in, for instance, electronics, pharmaceuticals, coating, personal and health care, and particularly the areas where heat-transfer enhancement[3–11] is required such as nuclear reactor cooling, engine cooling, fuel cells, and heat exchangers. It has been commonly known that to maintain the stability of nanoparticles in fluids, that is, to prevent those particles from aggregation, surface charges are normally required[12–17] to provide sufficient electrostatic repulsion[18,19] between the particles according to the Derjaguin, Landau, Verwey and Overbeek (DLVO) theory.[20,21]

Originated from von Smoluchowski,[22] the study of aggregation kinetics of colloidal nanoparticles has long been a central interest to scientists of nanoparticles.[1,23–25] It has to be mentioned that it was also originated from von Smoluchowski[22] that the population balance method has become a widely adopted approach for studying aggregation kinetics.[26–30] Nevertheless, except that, Feke and Schowalter[24] investigated rapid coagulation of nanoparticles for the cases based on Brownian diffusion and shear flow to find the dependence of system stability related net aggregation rate on system parameters. The core-shell method[1,25,31] has also made an impact on the diverse functionalities[32–36] of the nanoparticles. It has to be said that the aggregation status of the particles in a suspension determines the stability[23,24,37–45] and the properties[46,47] of the suspension.[12,24,25,45,48,49] Despite some studies on the stability ratio or the coagulation rate of nanoparticles using the fractal method[50–53] and the light scattering techniques,[41,54] it has still not been seen how the aggregation status can be quantified and how it can be related to the fundamental interactions between the particles.

Correspondence concerning this article should be addressed to L. Liu at l.liu@hud.ac.uk.

Van der Waals attraction[18] and the electrostatic repulsion were regarded as the main forces that dominate the interactions of the nanoparticles in fluids before Kruyt and De Jong's work[55] on hydration repulsion emerged. As clearly stated by Derjaguin[56] that the repulsive forces between colloidal particles should include the forces of the second kind in the absence of electrolytes. The origin of this kind was indicated to be solvation or hydration (solvation is a more general term including both hydrophobic attraction[57] and hydration repulsion[58] for hydrophobic and hydrophilic particles in aqueous suspensions, respectively; this article only refers to the latter) but at that time this was only qualitative and an awareness. It was then until 1970s, hydration force started receiving an increased attention[59–68] due to the fact that this force was observed to arise strongly with an exponential decay length of typically several Ås[60–62,64,69] especially in biological systems,[62,65,70] colloidal silica suspensions[59–61,71,72] and other environmental colloidal[73] and polymeric systems.[39,74] Some studies have been carried out recently with molecular dynamics simulations[75–77] of the structural hydration force, it has now become more and more clear that this force has an exponential decay over a characteristic length of the order of Å and plays a critical role in stabilizing hydrophilic nanoparticles in aqueous suspensions.[42,78,79] However, it is not clear how this force together with the electrostatic and van der Waals interactions is quantitatively connected to the aggregation of nanoparticles.

This article studies the aggregation of silica nanoparticles in an aqueous suspension in which the change of zeta potential takes place. It is to establish a quantitative relationship between the collision success factor – the aggregation coefficient and the interaction energies based on a kinetic theory of aggregation.[80] Much effort is given to the determination of the constants for the hydration repulsion and the calculation of the collision success factor. An inverse population balance technique[81–83] is used to extract the aggregation rate constants from the experimental particle size distributions (PSDs).

The Collision Success Factor

In kinetic theory of aggregation,[80] the collision success factor, $\psi_{\varepsilon v}$ (−), describes the probability of a collision between two particles of volume ε (m^3) and v (m^3) to succeed for an aggregate. In an overall perspective, it specifies the fraction of the successful collisions for aggregation between particles ε and v. This factor was given in an analytical form[80] for the case of no or negligible repulsion before two particles collides. However, for systems where particles undergo aggregation and have to overcome repulsion before they can collide and aggregate, the collision success factor for particles of volume ε and v is given by

$$\psi_{\varepsilon v}=(1+\theta_{\varepsilon v}{}^*/\theta_s)exp(-\theta_{\varepsilon v}{}^*/\theta_s) \quad (1)$$

where θ_s (J) is the ensemble average of the kinetic energy of all particles in the system and $\theta_{\varepsilon v}{}^*$ (J) is the repulsion energy — the critical relative kinetic energy (CRKE) of the collisions between particles ε and v. Equation 1 means any collisions between these two types of particles with a relative kinetic energy larger that $\theta_{\varepsilon v}{}^*$ would lead to aggregation. This critical energy is understood as the energy resulted from a balance between the attraction and repulsion forces in a collision.

According to the original kinetic theory,[84] θ_s is

$$3kT/2 \quad (2)$$

where k (J K^{-1}) is the Boltzmann constant and T (K) is the thermal temperature of the nanoparticles in the suspension. Also, for a system where particles are narrowly distributed in size as seen in Figure 2a of the experimental section of this article, Eq. 1 can then be approximated to

$$\psi=(1+2\theta_c/3kT)exp(-2\theta_c/3kT) \quad (3)$$

where $\theta^*_{\varepsilon v}$ of Eq. 1 has been replaced by θ_c (J) for all the particles.

The Critical Relative Kinetic Energy

The CRKE is defined as the energy at which a balance between the attraction and repulsion forces on a particle in a collision is reached.[80] However, in the case of aggregation, such a balance also refers to the equilibrium between the monomers (the colliding particles) and the dimers (the aggregated particles). In systems of hydrophilic nanoparticles suspended in water where particles are also surface charged, the attraction energy between those particles is attributed to the van der Waals attraction,[60,85] while the repulsion energy between the particles is given by the sum of the electrostatic[86] and the hydration potential energies.[64,71] As also discussed by Hiemenz[86] and will be seen latter in this article from Figure 6b, the force balance refers to the peak of the net potential energy curve which is thermodynamically unstable so does not necessarily produce a stable aggregate; while at the separation distance where a zero net energy is reached, a stable aggregate would be considered to have formed as any approaching contact closer than that the net energy would become entirely attractive indicating a no escape between the aggregating monomers. Therefore, the CRKE in this article refers to either the attraction or the repulsion energy when the sum of them is zero and the separation distance between the two monomers at this point refers to the equilibrium distance, s_{eq}.

The attraction energy between two particles is given by

$$-Al/24s \quad (4)$$

where A (J) is the Hamaker constant, l (m) is the particle size in diameter, and s (m) is the surface separation distance between two contacting particles. The negative sign denotes attraction. Note, Eq. 4 is a simplified form of the van der Waals attraction potential[86] with a uniform particle size l (an average of the mean sizes in this article) and $l >> s$.

The electrostatic repulsion between two particles according to the DLVO and the Gouy-Chapman theories[86] can be written as

$$\frac{32\pi lcRT}{\kappa^2}\mathrm{Tanh}^2\left(\frac{zF\Psi_0}{4RT}\right)\exp(-\kappa s) \quad (5)$$

where c (mol m^{-3}) is the total molar concentration of the ions in the suspension, R (J K^{-1} mol^{-1}) is the gas constant, T (K) is the thermal temperature, F (C mol^{-1}) is the Faraday constant, z (–) is the valence of ions in suspension, and Ψ_0 (V) is the electrical potential on the surface of the particles. κ^{-1} (m) is the "thickness" of the double layer and can be calculated as $[\varepsilon_0\varepsilon_r RT/(2F^2I)]^{1/2}$ where ε_0 (F m^{-1}), ε_r (–), and I (mol m^{-3}) are the dielectric constant of vacuum, relative dielectric constant of the medium, and the ionic strength of the electrolytes in the suspension, respectively.

The hydration repulsion between two particles is written as

$$\Phi_0 \exp(-\lambda s) \quad (6)$$

where Φ_0 (J) is a constant and λ^{-1} (m) is the characteristic length of the exponential decay.

When the sum of the attraction and repulsion energies is 0, combining Eqs. 5 and 6 with Eq. 4 yields

$$\frac{32\pi lcRT}{\kappa^2}\mathrm{Tanh}^2\left(\frac{zF\Psi_0}{4RT}\right)\exp(-\kappa s)+\Phi_0\exp(-\lambda s)=\frac{Al}{24s} \quad (7)$$

Taking approximations: $\mathrm{Tanh}\left(\frac{zF\Psi_0}{4RT}\right)\rightarrow\frac{zF\Psi_0}{4RT}$, $\exp(-\kappa s)\rightarrow 1-\kappa s$, and $\exp(-\lambda s)\rightarrow 1-\lambda s$, Eq. 7 can be solved to give a valid analytical solution of s as s_{eq}

$$s_{eq}=\frac{6RT\Phi_0\kappa^2+12\pi lcF^2z^2\Psi_0{}^2-[36(RT\Phi_0\kappa^2+2\pi lcF^2z^2\Psi_0{}^2)^2-6AlRT\kappa^3(RT\Phi_0\kappa\lambda+2\pi lcF^2z^2\Psi_0{}^2)]^{1/2}}{12\kappa(RT\Phi_0\kappa\lambda+2\pi lcF^2z^2\Psi_0{}^2)} \quad (8)$$

As the equilibrium distance should be greater than 0, that is, $s_{eq}\geq 0$, Φ_0 has to satisfy

$$\Phi_0 \geq l\times\frac{ART\lambda\kappa^2-24\pi cF^2z^2\Psi_0{}^2+\kappa\{ART[ART\kappa^2\lambda^2+48\pi cF^2z^2\Psi_0{}^2(\kappa-\lambda)\}^{1/2}}{12RT\kappa^2} \quad (9)$$

Table 1. The Properties of ST50 and Parameters Used for the Evaluation of θ_c

Hamaker Constant for Silica, A (J)	Vacuum dielectric constant, ε_0 (F m^{-1})	Relative dielectric constant of medium, ε_r (F m^{-1})	Boltzmann constant, k (J K^{-1})	Faraday constant, F (C mol^{-1})	Total molar concentration of ions, c (mol m^{-3})
0.46×10^{-20}	8.85×10^{-12}	80	1.38×10^{-23}	9.65×10^{4}	534.19[a]
Ionic strength, I (mol m^{-3})	Valence, z	Gas constant, R (J K^{-1} mol^{-1})	Particle size, l (m)	Debye length, κ^{-1} (m)	Viscosity of the medium, μ (mPa s)
267.10[a]	1	8.31	1.22×10^{-8}[b]	5.94×10^{-10}[c]	50

[a]Based on 0.6%wt NaOH.
[b]Average of the 1–0 mean sizes.
[c]Calculated according to $[\varepsilon_0\varepsilon_r RT/(2F^2I)]^{1/2}$
The temperature, $T = 298$ K.

For a nanosuspension where the particles are not surface charged and electrolyte is absent, that is, $\Psi_0 = 0$, $c = 0$, $z = 0$, and $\kappa^{-1} = 0$ namely $\kappa \to \infty$, Eq. 9 can be simplified to become

$$\Phi_0|_{\Psi_0=0} \geq \frac{lA\lambda}{6} \tag{10}$$

where $\Phi_0|_{\Psi_0=0}$ denotes Φ_0 at $\Psi_0=0$. This suggests that the lower limit of the hydration repulsion constant can be estimated according to Eq. 10, which requires only the knowledge of λ.

Substituting Eq. 8 into Eq. 4 with the negative sign eliminated as the CRKE is only concerned with the magnitude of the energy, we have

$$\theta_c = \frac{Al(\lambda\Lambda^2+\kappa\Psi_0{}^2)}{12\left\{(\Lambda^2+\Psi_0{}^2)-\left[(\Lambda^2+\Psi_0{}^2)^2-\frac{ART\kappa^2(\lambda\Lambda^2+\kappa\Psi_0{}^2)}{12\pi cz^2F^2}\right]^{1/2}\right\}} \tag{11}$$

where Λ is defined as

$$\Lambda = \left(\frac{RT\Phi_0\kappa^2}{2\pi lcz^2F^2}\right)^{1/2} \tag{12}$$

It is clear that Λ has a unit of Voltage.

With $\kappa = \left(\frac{2F^2I}{\varepsilon_0\varepsilon_r RT}\right)^{1/2}$, Eq. 12 can be changed to

$$\Lambda = \left(\frac{\Phi_0 I}{\pi lc\varepsilon_0\varepsilon_r z^2}\right)^{1/2} \tag{13}$$

Λ is thus understood as equivalent to the electrical potential when the hydration repulsion at the surface of the particles is converted into the electrostatic energy at the local electrolyte environment.

A further simplification can be made to Eq. 13 if the medium environment is 1:1 electrolyte as the case in this article. The ionic strength is then $I = \frac{1}{2}\sum_{i=1}^{2} c_i z_i{}^2 = \frac{1}{2}\sum_{i=1}^{2} c_i = \frac{c}{2}$, where i (–) is the number of the ion types, c_i (mol m^{-3}), and z_i (–) are their corresponding mole concentration and valence, respectively. Equation 13 can then be changed to

$$\Lambda|_{1:1} = \left(\frac{\Phi_0}{2\pi l\varepsilon_0\varepsilon_r}\right)^{1/2} \tag{14}$$

where $\Lambda|_{1:1}$ denotes Λ at a 1:1 electrolyte.

In the case that the double layer exists and the particle radius is much greater than the thickness of the double layer, that is, $l \gg \kappa^{-1}$ (as seen in Table 1), Ψ_0 can be replaced by the zeta potential at the diffusion layer,[12,13,19] $\Psi_0 \approx \zeta$, Eq. 11 would then become

$$\theta_c = \frac{Al(\lambda\Lambda^2+\kappa\zeta^2)}{12\left\{(\Lambda^2+\zeta^2)-\left[(\Lambda^2+\zeta^2)^2-\frac{ART\kappa^2(\lambda\Lambda^2+\kappa\zeta^2)}{12\pi cz^2F^2}\right]^{1/2}\right\}} \tag{15}$$

It should be noted that Λ and ζ appeared in Eq. 15 with a same second order and similar coefficients. This suggests that both Λ and ζ affect the calculation of θ_c and consequently the aggregation coefficient according to Eq. 3 in a similar way but independent of each other. s_{eq} expressed by Eq. 8 can as well be changed to

$$s_{eq} = \frac{\Lambda^2+\zeta^2-\left[(\Lambda^2+\zeta^2)^2-\frac{ART\kappa^2(\lambda\Lambda^2+\kappa\zeta^2)}{12\pi cz^2F^2}\right]^{1/2}}{2(\lambda\Lambda^2+\kappa\zeta^2)} \tag{16}$$

The Aggregation Rate Constant

A population balance analysis is used to extract the aggregation rate constants based on the Moment method[82,83] and a discretization technique[81] with the use of the measured nanoparticle size distributions. A brief discussion of this method and the numerical technique is given below.

The population balance equation for nanoparticle aggregation in a well-mixed system with the change of zeta potential monitored can be written as

$$\frac{\partial n(\zeta,v)}{\partial\zeta} = \frac{1}{2}\int_0^v \beta(\zeta,\varepsilon,v-\varepsilon,)n(\zeta,\varepsilon)n(\zeta,v-\varepsilon)d\varepsilon - n(\zeta,v)\times\int_0^\infty \beta(\zeta,\varepsilon,v)n(\zeta,\varepsilon)d\varepsilon \tag{17}$$

where n (m^{-6}) is the number density of the particles. β (m^3 V^{-1}) is the so called aggregation kernel and is a function of particle size and ζ. On the right-hand side of Eq. 17, the first term is called the "birth rate" — the rate of the collisions between particles of volume ε and $v-\varepsilon$ resulting in the "birth" of the particles of v. The second term is called the "death rate"—the rate of the collisions between particles v and any size of particles leading to the "death" of the particles v.

According to von Smoluchowski[22] for particles undergoing Brownian motion, the aggregation kernel can be expressed as

$$\frac{2kT}{3\mu}(\varepsilon^{1/3}+v^{1/3})(\varepsilon^{-1/3}+v^{-1/3}) \tag{18}$$

where μ (Pa s) is the viscosity of the continuous phase in the suspension and k (J K^{-1}) is the Boltzmann constant.

However, not all the collisions lead to aggregation, the collision success factor that quantifies the successful aggregations should be applied.[80] Thus

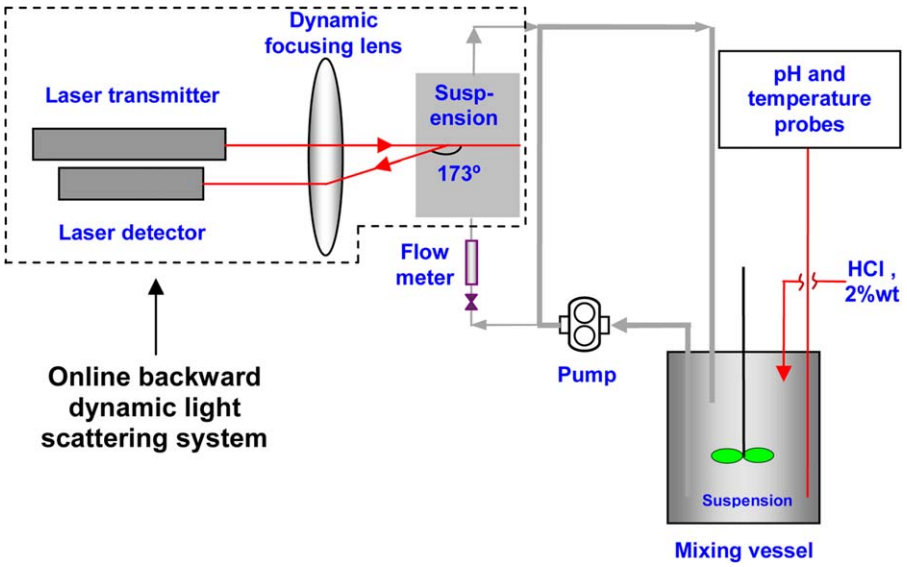

Figure 1. The schematic representation of the experimental setup.

[Color figure can be viewed in the online issue, which is available at wileyonlinelibrary.com.]

$$\beta(\zeta,\varepsilon,v)=\psi(\zeta)\frac{2kT}{3\mu}(\varepsilon^{1/3}+v^{1/3})(\varepsilon^{-1/3}+v^{-1/3}) \tag{19}$$

A size dependent function $f(\varepsilon,v)$ (–) and a rate constant $\beta_0(\zeta)$ ($m^3\ V^{-1}$) of the aggregation kernel can then be defined as

$$f(\varepsilon,v)=(\varepsilon^{1/3}+v^{1/3})(\varepsilon^{-1/3}+v^{-1/3}) \tag{20}$$

$$\beta_0(\zeta)=\psi(\zeta)\frac{2kT}{3\mu} \tag{21}$$

In Eq. 21, the analytical form of $\psi(\zeta)$ is given by Eq. 3 where θ_c takes the expression of Eq. 15.

In the extraction of the rate constants from PSDs, the Moment method[82] transforms Eq. 17 into a Moment form by integrating its both sides over the range of v from 0 to ∞. Taking Eqs. 20 and 21 into consideration, Eq. 17 can thus become

$$\frac{\partial n(\zeta,v)}{\partial\zeta}=\beta_0(\zeta)$$

$$\left(\frac{1}{2}\int_0^v f(\varepsilon,v-\varepsilon,)n(\zeta,\varepsilon)n(\zeta,v-\varepsilon)d\varepsilon-n(\zeta,v)\int_0^\infty f(\varepsilon,v)n(\zeta,\varepsilon)d\varepsilon\right)$$

$$=\beta_0(\zeta)[B(\zeta,v)-D(\zeta,v)] \tag{22}$$

where $\int_0^v f(\varepsilon,v-\varepsilon)n(\zeta,\varepsilon)n(\zeta,\varepsilon-v)d\varepsilon=B(\zeta,v)$ and $n(\zeta,v)\int_0^\infty f(\varepsilon,v)\ n(\zeta,\varepsilon)d\varepsilon=D(\zeta,v)$.

$B(\zeta,v)-D(\zeta,v)$ can then be calculated using a numerical technique[81] that discretises the entire particle size range into a series of intervals with a progression of $^1/_2$ in volume size from the small to its neighbouring large ones. This technique transforms Eq. 22 into a series of ordinary equations in terms of the discretised sizes so that the numerical solution of the number density of the particles in each size interval can be numerically solved

$$B(\zeta,v_q)-D(\zeta,v_q)\cong N_{p-1}\sum_{q=1}^{p-2}2^{q-1+p}f_{p-1,q}N_q$$

$$+\frac{1}{2}f_{p-1,q-1}{N_{p-1}}^2-N_p\sum_{q=1}^{p-1}2^{q-1}f_{p,q}N_q-N_p\sum_{q=1}^{n_{eq}}f_{p,q}N_q \tag{23}$$

where the subscripts p and q denote the discretised size intervals and n_{eq} means the largest sequence number of the discretised size intervals and is determined by $\frac{\ln(v_{max}/v_{min})}{\ln 2}+1$ where v_{max} and v_{min} are the maximum and minimum particle volume sizes from experiment, respectively. N (m^{-3}) represents the number of the particles per unit volume in the denoted size intervals by its subscript.

Multiplying $v^{j/3}$ to both sides of Eq. 22 and integrate it over v from 0 to ∞, we then have

$$\int_0^\infty v^{j/3}\frac{\partial n(\zeta,v)}{\partial\zeta}dv=\frac{dm_j(\zeta)}{d\zeta}=\beta_0(\zeta)\int_0^\infty v^{j/3}[B(\zeta,v)-D(\zeta,v)]dv$$

$$\approx\beta_0(\zeta)\sum_{q=1}^{n_{eq}}v_q{}^{j/3}[B(\zeta,v_q)-D(\zeta,v_q)] \tag{24}$$

where the jth Moment: m_j, is defined as $\int_0^\infty v^{j/3}n(v)dv$ with $j=0,\ 1,\ 2,\ 3,\ 4$. It is clear that m_0 (m^{-3}) and m_1 (m^{-2}) represent the total number and length of the particles per unit spatial volume, respectively; m_2 (m^{-1}) and m_3 (–) correspond to the total surface area and total volume of the particles per unit spatial volume when appropriate particle shape factor is applied, respectively. The aggregation rate constant $\beta_0(\zeta)$ can be obtained by

$$\beta_0(\zeta)=\frac{\Delta m_j(\zeta)/\Delta\zeta}{\sum_{q=1}^{n_{eq}}v_q{}^{j/3}[B(\zeta,v_q)-D(\zeta,v_q)]} \tag{25}$$

It should be pointed out that as the calculation of $dm_j(\zeta)/d\zeta$ is approximated by $\Delta m_j(\zeta)/\Delta\zeta$ in Eq. 25, the step size $\Delta\zeta$ can affect the accuracy of the estimated $\beta_0(\zeta)$ if $m_j(\zeta)$ is not linearly related to ζ. It is generally true that more ζ points and smaller step size $\Delta\zeta$ would give a more accurate estimation of $\beta_0(\zeta)$. The experiment presented in this article as seen in the next section has nine ζ points measured. It can also been seen from Figure 3 that the measured ζ points are more concentrated in the region (from -15.6 to -4.66 mV) where a dramatic change of $\beta_0(\zeta)$ has taken place, it can thus be said that the number of the measured ζ points has provided to a large extent a sufficient information for representing the trend of $\beta_0(\zeta)$.

The whole method described in this section for obtaining the aggregation rate constants, in the last section for

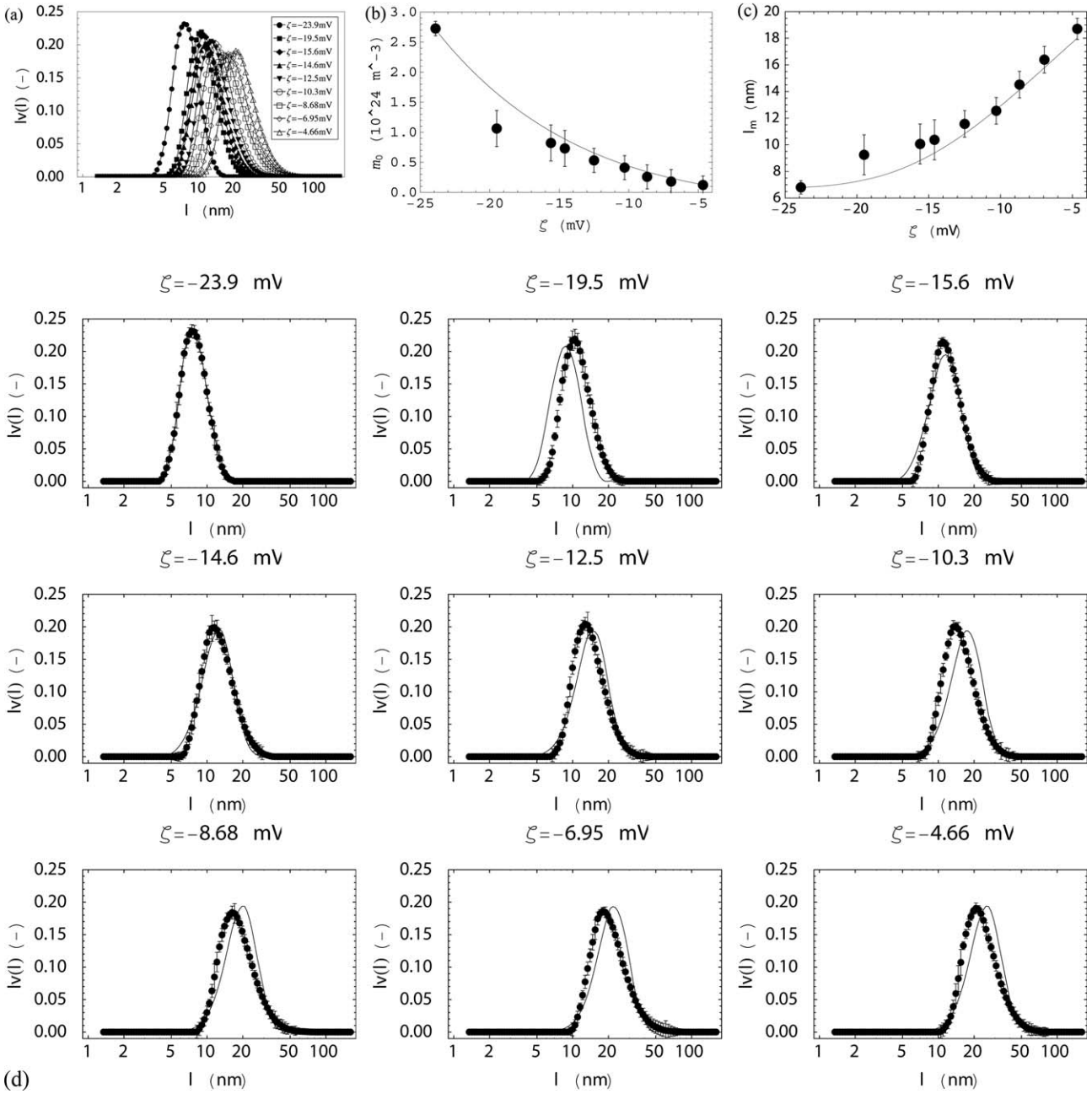

Figure 2. (a) The experimental results of the change of the nanoparticle size distribution with ζ, (b) The total number of the particles m_0, (c) The 1–0 mean sizes, and (d) The comparison of the volume fractions of the particles between the population balance simulation and the experimental measurement.

Note, in (b), (c), and (d), the dots and lines are for the experiment and the simulation, respectively. The error bars indicate the accuracy of experimental measurements. l (nm), $v(l)$ (nm^{-1}), and l_m (nm) denote the particle size in diameter, the volume density of the particles of diameter l, and the mean size, respectively.

calculating the CRKE and in a previous section on collision success factor can now be integrated together to develop an inverse technique to determine Φ_0 and λ for the hydration repulsion. First, calculate $\beta_0(\zeta)$ from the experimental PSDs based on Eq. 25; second, using Eq. 21 to calculate the collision success factor $\psi(\zeta)$; and finally according to the analytical form of $\psi(\zeta)$ in Eq. 3 and the CRKE θ_c in Eq. 15, using nonlinear model regression techniques such as minimising the sum of squares to best fit the data of $\psi(\zeta)$ to determine Φ_0 and λ.

Experimental

Materials and setup

The experiment was designed to demonstrate the aggregation of nanoparticles in a liquid by changing zeta potential. The materials used in this experiment were a silica nanoparticle suspension (SNOWTEX ST50, Nissan Chemicals, America Co.) and a 2.0%wt HCl solution for titration. The SNOWTEX ST50 is colloidal silica made by growing monodispersed, negatively charged silica particles in water.

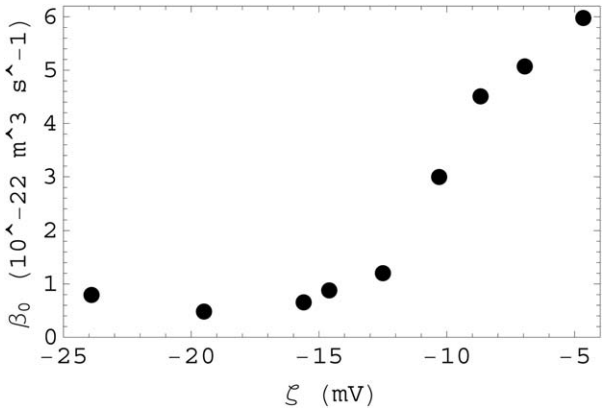

Figure 3. The extracted aggregation rate constants β_0 changing with ζ.

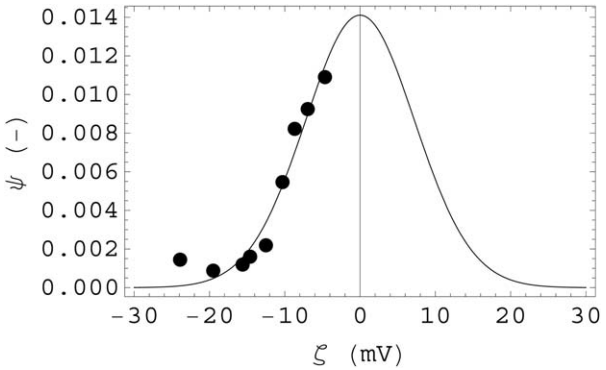

Figure 4. The collision success factor.

Note, the dots are the data calculated from the extracted aggregation rate constants and the curve is plotted using $\psi=(1+2\theta_c/3kT)\ \exp\ (-2\theta_c/3kT)$ with $\Phi_0 = 4.93 \times 10^{-20}$ and $\lambda = 3.61 \times 10^9$ for θ_c in Eq. 15.

$[OH]^{-1}$ ions exist at the surface of the particles with an electrical double layer formed by alkali ions. Stabilization is achieved by the repulsion between the same negatively charged particles. The key properties of ST50 are listed in Table 1.

The experiment was carried out at a temperature of 25°C in a 500 mL vessel that was connected to an online backward light scattering instrument[87,88] (Malvern Instruments Plc) for the real time measurement of zeta potential and size distribution of the nanoparticles. The suspension flow was driven by a positive displacement pump and monitored by a pH and temperature probe. A small agitator was used to facilitate the mixing of HCl in the vessel with the suspension and to ensure that the suspension was well-mixed before measurements were taken. The schematic structure of the experimental rig is illustrated in Figure 1.

The experimental results

Figure 2 shows the change of the PSD with ζ (Figure 2a) and their corresponding total number of particles: m_0 (dots in Figure 2b) and mean sizes l_m (m_1/m_0, dots in Figure 2c). It is clear from this figure that the nanoparticles have experienced a process of progressive aggregation.

The Modelling Results

The modelling procedure is described as follows.

First, use the zeroth Moments calculated from the measured size distributions of the nanoparticles at different ζ (shown in Figure 2a) to extract the aggregation rate constants according to Eq. 25.

Second, use the extracted aggregation rate constants to carry out a forward population balance simulation to compute the theoretical PSDs and compare them with the experimentally measured ones (Figure 2a) to justify the extracted rate constants.

Finally, convert those rate constants into the numerical values of the collision success factor at different ζ according to Eq. 21 and use the analytical expression of ψ in Eq. 3 with the mathematical form of θ_c in Eq. 15 and the NonlinearModelFit built-in on Mathematica 9.0 (Wolframe Research Inc.) to determine Φ_0 and λ for the hydration repulsion.

The extracted aggregation rate constants and the population balance modelling results

Figure 3 shows the extracted aggregation rate constants and it is clear from this figure that with the decrease of the magnitude of ζ the rate constant increases, which suggests a weakening repulsion.

Figure 2d shows the comparison of the volume fractions of the nanoparticles between the experimental (dots) and the population balance simulation (lines); the size distribution corresponded total number and mean size of the particles are shown in Figures 2b and c (in both figures, dots are experimental and lines are modelling), respectively. It is clear from Figure 2b–d that the population balance model based simulation results are largely in agreement with the experimental data. This justifies the method to obtain the aggregation rate constants and suggests that these constants can be taken for the calculation of the collision success factor.

The hydration repulsion constant and the characteristic length of the exponential decay

According to Eq. 21, divided by $2kT/3\mu$, the extracted aggregation rate constants can be converted into the collision success factor, as the numerical value of $2kT/3\mu$ does not change with ζ, the plot of ψ against ζ thus has a same shape as Figure 3.

It is expected that Eq. 3 is able to describe the theoretical relationship between ψ and ζ with Eq. 15 for the evaluation of θ_c. In Eq. 15, except for λ and Φ_0 (included in Λ in Eqs. 12–14) other parameters are calculated and given in Table 1. Based on Eq. 3 and those parameters in Table 1, the best fit to the collision success factor data generated $\Phi_0 = 4.93\ 10^{-20}$ (J) and $\lambda = 3.61 \times 10^9$ (m^{-1}), that is, $\lambda^{-1} = 2.77 \times 10^{-10}$ (m). The regression statistics are given in Table 2.

As seen from Table 2, that the confidence level of the nonlinear fit was 99%, the extremely small P-Values for both Φ_0

Table 2. The Statistics of the Regression for Φ_0 and λ

	Estimate	Standard Error	t Statistic	P-Value	R^2	Confidence Level	Parameter Confidence Intervals
Φ_0	4.93×10^{-20}	3.44×10^{-22}	143.54	2.10×10^{-13}	0.98	0.99	$(4.81 \times 10^{-20}, 5.06 \times 10^{-20})$
λ	3.61×10^{9}	1.19×10^{-51}	3.02×10^{60}	1.14×10^{-421}			$(3.61 \times 10^{9}, 3.61 \times 10^{9})$

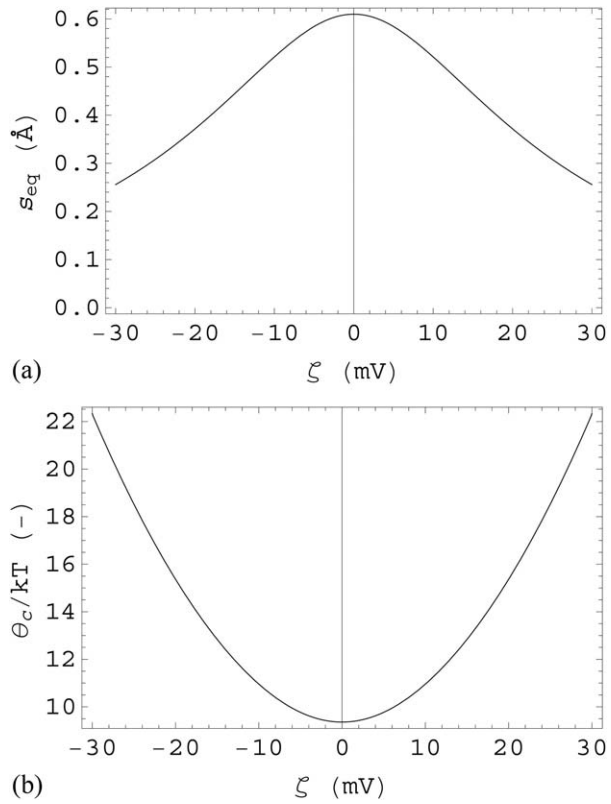

Figure 5. (a) The equilibrium distance s_{eq} changing with ζ. (b) The CRKE, θ_c/kT changing with ζ.

and λ reject the null hypothesis: zero coefficients, $R^2 = 0.98$ and the parameter confidence intervals especially that for λ confirms the goodness of the fit and justifies the two constants. It is important to point out that the two constants strongly agree with that suggested in literature.[61,62,64,65,75,89,90]

Figure 4 shows a comparison between the success factor data (dots) and the theoretical relationship expressed in Eq. 3 and it can be seen from this figure, when $\zeta = 0$, $\psi = 0.014$. This suggests that in an aqueous suspension of silica nanoparticles, if the particles are not surface charged and electrolytes are not present, due to only the hydration repulsion, the probability of two colliding particles to succeed for an aggregate is about 1.4% and among all the collisions taking place in the system, around 1.4% of them would succeed for aggregates. It can also be calculated according to Eq. 3, when the magnitude of $\zeta = 30$ mV, the collision success factor is approximately 5.5×10^{-6}.

The Equilibrium Distance, the Critical Relative Kinetic Energy and the Hydration Repulsion

The equilibrium distance and the critical relative kinetic energy

The equilibrium distance is the surface separation distance between two colliding particles when the sum of their repulsion and attraction energies have reached zero. Its solution is given by Eq. 16. This distance depends on ζ as it affects the electrostatic repulsion and is shown in Figure 5a. The CRKE, represented by Eq. 15, divided by kT is shown in Figure 5b.

It is seen from Figure 5a, with the increase of the magnitude of ζ, s_{eq} approaches 0, which indicates that the aggregation between particles becomes more and more difficult. This is because according to Eq. 4, a small s_{eq} will produce a large θ_c, ψ will then become small according to Eq. 3 thus reduces the chance of the successful aggregations. In Figure 5b, the point of θ_c/kT at $\zeta = 0$ (the lowest point on the curve) corresponds to the case when the hydration repulsion is the only repulsion that balances the van der Waals attraction and its corresponding equilibrium separation distance as shown in Figure 5a is approximately 0.6 Å.

The hydration repulsion

The hydration repulsion now expressed as $\Phi = 4.93 \quad 10^{-20} \exp(-3.61 \times 10^9 s)$, divided by the thermal energy (kT) of the nanoparticles in the suspension, is shown in Figure 6a (the line with $\zeta = 0$).

The exponential decay length λ^{-1} is calculated to be 2.77 Å – less than half of the Debye length ($\kappa^{-1} = 5.94$ Å given in Table 1) suggests that the hydration repulsion is a shorter range interaction than the electrostatic repulsion.

Figure 6a also shows a comparison between the van der Waals attraction, the hydration ($\zeta = 0$) and the electrostatic repulsions for $\zeta = -30$, -20, and -10 mV. It can be seen from this figure, compared to the electrostatic repulsion at $\zeta = -30$ mV, the hydration repulsion appears to be stronger when the separation distance is shorter than approximately 0.5 Å.

Figure 6b shows the sum of the van der Waals attraction, the electrostatic and the hydration repulsions. It is clear from

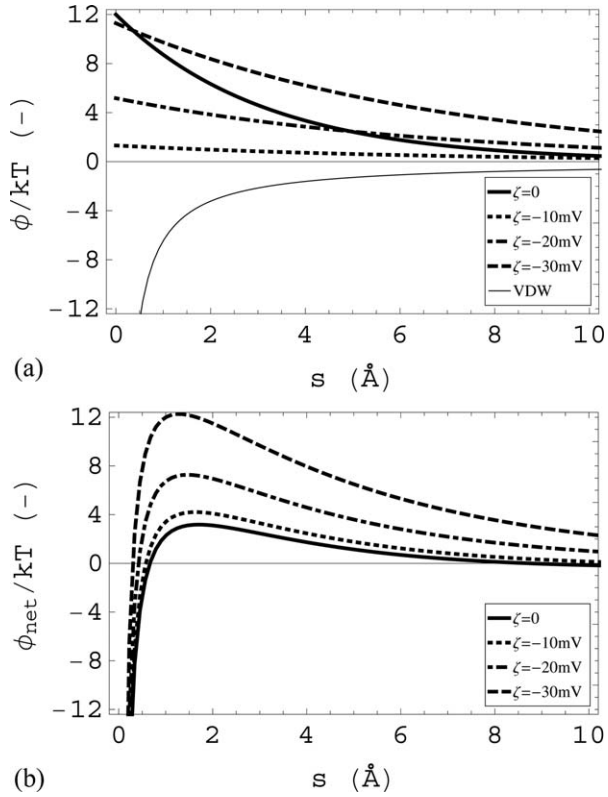

Figure 6. The comparison between the van der Waals attraction, the hydration and the electrostatic repulsions where φ (J) represents in general the energy and s (Å) denotes the separation distance between the surfaces of the particles.

φ_{net} means the net potential energy. (a) The individual energies and (b) the sum of the energies. Note, in the legends, $\zeta = 0$ refers to the hydration repulsion only but in (b) this means the sum of the attraction and hydration repulsion only.

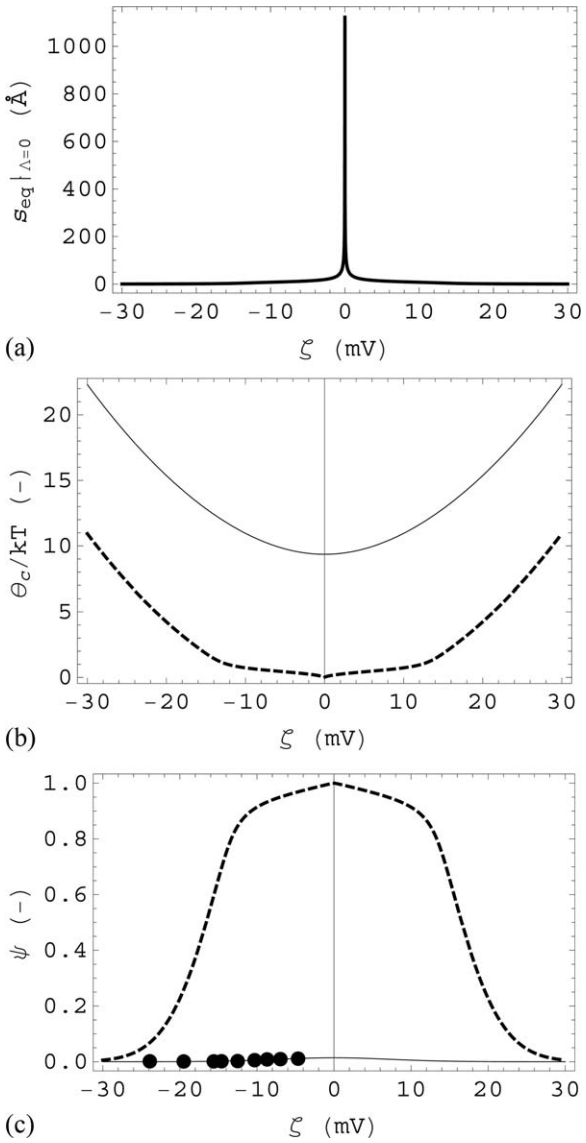

Figure 7. (a) The equilibrium distance s_{eq} at $\Lambda = 0$. (b) and (c) are the comparisons for θ_c and ψ between $\Lambda = 0$ (the dashed lines) and $\Lambda = 30$ mV (the solid lines), respectively. Note, in (c), the solid line with dots has been shown in Figure 4.

this figure that if particles are not surface charged and there are no electrolytes in the suspension, that is, $\zeta = 0$, for two particles to become aggregated, they have to overcome a basic energy barrier that is approximately $3.2kT$ attributed to the hydration repulsion.

As λ is now determined and indeed in the range of several Ås, the right-hand side of Eq. 10 can be calculated to be 3.39×10^{-20} (J), approximately $8.24kT$, which is a rather good estimate to the determined $\Phi_0 = 4.93 \times 10^{-20}$ (J), approximately $12kT$. This means that Eq. 10 can be used to calculate an initial numerical value of Φ_0 for the nonlinear regression of the ψ data to determine Φ_0 and λ.

The Hydration Potential

Λ, given by Eq. 13, regarded as an equivalent electrical potential at the surface of the nanoparticles when the hydration repulsion is converted into the electrostatic energy, is calculated to be ± 30 mV. With λ^{-1} being less than half of κ^{-1}, this suggests that Λ can be essentially considered as an additional potential to the double layer electrostatic potential at the stem surface of the nanoparticles, to name it: the hydration potential. It is additional to and independent of the electrostatic potential as shown in Eqs. 15 and 16.

Compared to the recognition that normally a magnitude of 30 mV[56,91] of ζ would be able to stabilise a hydrophilic aqueous colloidal system, this calculated $\Lambda = \pm 30$ mV is thought to be a rather strong potential additional to ζ. If without this hydration potential, that is, $\Lambda = 0$, the equilibrium distance $s_{eq}|_{\Lambda=0}$, is shown in Figure 7a.

It is seen from Figure 7a, when $\zeta = 0$, $s_{eq}|_{\Lambda=0} \rightarrow \infty$. This means when the electrostatic repulsion is effectively 0 and if the hydration repulsion does not exist, according to Eq. 7 the only way for the van der Waals attraction to be "balanced" is that the equilibrium distance becomes ∞.

A comparison for the CRKE θ_c/kT between $\Lambda = 0$ and $\Lambda = 30$ mV can also be made and is shown in Figure 7b. It is clear from Figure 7b, the difference between these two lines is the hydration repulsion at $s_{eq} = 0.6$ Å, approximately $9.4kT$. For $\theta_c|_{\Lambda=0}$ (the dashed line), when $\zeta = 0$, it is 0 (the lowest point), which suggests that the collision success factor has reached the maximum value: 1 as indeed seen from Figure 7c (the dashed line). This is because at this ζ point the total repulsion is 0 all the collisions would succeed for aggregation.

As seen from Figure 7c, without the hydration potential, the collision success factor could become considerably larger than that with the hydration potential and for a same collision success factor, that would require a much higher double layer electrostatic potential. For instance, with $\Lambda = 30$ mV and $\zeta = 30$ mV, $\psi = 5.5 \times 10^{-6}$; however, to achieve the same ψ value if Λ=0, ζ should be 42 mV. This means that a 30 mV hydration potential is equivalent to a 12 mV electrostatic potential and the contribution from the hydration potential to the collision success factor in preventing the particles from aggregation is 29% in a 30 mV zeta potential system.

Based on the above discussion, it follows that a suggestion of a figure of 10^{-6} collision success factor may be made as a criterion to justify a relatively stable suspension. This figure corresponds to an equilibrium distance of 0.23 Å, a 33 mV zeta potential in addition to a 30 mV hydration potential.

It is worth pointing out that it is the mathematical form Eq. 1 of the collision success factor that laid the foundation for the whole approach to work. It created a link between particle interaction energies and aggregation rate constant. The method itself does not have limitation as far as the determination of the hydration repulsion constants concerns as long as the PSD can be measured accurately.

It should be commented that Eq. 1 was derived from a normalized relative velocity distribution function,[80] which has eliminated the effect of particle concentration and collision mechanism. Nevertheless, because the normalized velocity distribution function was based on Maxwell's distribution, if the velocity distribution of particles in a fluid system deviated far away from Maxwell's, then Eq. 1 may become problematic. However, for most particle-fluid systems, the velocity distribution of particles still follows the Maxwell's or can be described by higher orders (mostly a second order would be sufficient) of the Chapman-Enskog approximation[92] which is still based on the Maxwell's

distribution, then the validity of the mathematical form Eq. 1 will still largely hold.

It is interesting to mention that there are studies on the temperature dependence[93,94] of the hydration repulsion but this is not the scope of this article.

Conclusions

The hydration repulsion is found to have an equivalent electrical potential of 30 mV in magnitude at the stem surface of the silica nanoparticles and a 2.77 Å exponential decay length that is less than the Debye length and suggests that the hydration repulsion is a shorter range interaction than the electrostatic repulsion. In the silica system studied, the hydration repulsion contributes equivalently a 12 mV electrostatic potential in addition to the 30 mV zeta potential and accounts for 29% in forming the collision success factor to prevent the nanoparticles from aggregation. Due to this inherent approximately 3.2*kT* hydration repulsion in hydrophilic silica nanoparticle suspensions, the maximum aggregation coefficient of the particles is approximately 1.4%. It should also be pointed out that it is the collision success factor that justifies the relative stability of a nanoparticle suspension neither the hydration potential nor the zeta potential. 10^{-6} may become a useful figure for collision success factor to justify a relatively stable suspension. However, zeta potential combined with the hydration potential can be used to quantitatively manipulate the aggregation efficiency of the nanoparticles as to provide a way for the stability control of the hydrophilic nanoparticles in aqueous suspensions.

Notation

A = Hamaker constant, J
B = size dependence birth of particles, m^{-9}
c = total molar concentration of the ions in the suspension, mol m^{-3}
D = size dependence death of particles, m^{-9}
f = size dependence function in aggregation kernel, (–)
F = Faraday constant, C mol^{-1}
I = ionic strength, mol m^{-3}
k = Boltzmann constant, J K^{-1}
l = particle size in diameter, m
l_m = particle mean size in diameter, m
m_j = jth moment, m^{j-3}
n = particle number density, m^{-6}
n_{eq} = largest sequence number of the discretised size intervals, (–)
N = number of particles per unit volume in a discretised size interval by subscript, m^{-3}
p, q = discretised particle size intervals, (–)
R = gas constant, J K^{-1}
s = surface separation distance between particles, m
s_{eq} = equilibrium separation distance between particles, m
$s_{eq}|_{\Lambda=0}$ = equilibrium separation distance between particles when $\Lambda = 0$, m
T = thermal temperature, K
v = size of individual particles in volume, m^3
$v(l)$ = volume density of the particles of diameter l, m^{-1}
v_{max} = largest particle volume size from experiment, m^3
v_{min} = smallest particle volume size from experiment, m^3
z = valence of ions, (–)

Greek letters

β = aggregation kernel, m^3 V^{-1}
β_0 = aggregation kernel rate constant, m^3 V^{-1}
ε = size of individual particles in volume, m^3
ε_r = relative dielectric constant of a medium, F m^{-1}
Φ = hydration repulsion, J
Φ_0 = hydration repulsion constant, J
$\Phi_0|_{\Psi_0=0}$ = Φ_0 at zero surface charge: the lower limit of Φ_0 for its initial estimate, J
κ = double layer exponential decay constant, m^{-1}
λ = exponential decay constant of hydration repulsion, m^{-1}
Λ = equivalent electrical potential of hydration repulsion at the surface of a particle, V
$\Lambda|_{1:1}$ = Λat 1:1 electrolyte, V
μ = viscosity of the continuous phase, Pa s
ψ = collision success factor, (–)
$\psi_{\varepsilon v}$ = collision success factor between particles of volume size ε and ε, (–)
θ_c = critical relative kinetic energy, J
$\theta_c|_{\Lambda=0}$ = critical relative kinetic energy when $\Lambda = 0$, J
θ_s = ensemble average kinetic energy of particles, J
$\theta^*_{\varepsilon v}$ = critical relative kinetic energy between particles of volume size ε and ε, J
Ψ_0 = electrical potential on the surface of the particles, V
ζ = Zeta potential, V

Literature Cited

1. Caruso F. Nanoengineering of Particle Surfaces. *Adv Mater*. 2001; 13(1):11–22.
2. Pelizzetti E, editor. *Fine Particles Science and Technology: From Micro to Nanoparticles*. Dordrecht, Boston,London: Kluwer Academic Publishers, 1996.
3. Buongiorno J. Convective Transport in Nanofluids. *Trans ASME*. 2006;128:240–250.
4. Buongiorno J, Hu L-W. Nanofluid coolants for advanced nuclear power plants. *Paper presented at Proceedings of ICAPP '052005*; Seoul, May 15–19, 2005.
5. Choi SUS. Enhancing thermal conductivity of fluids with nanoparticles. In: Siginer DA, Wang HP, editors. *Developments and Applications of Non-Newtonian Flows*. ASME, FED-Vol. 231/MD-Vol. 66; 1995:99–105.
6. Choi SUS, Zhang ZG, Yu W, Lockwood FE, Grulke EA. Anomalous thermal conductivity enhancement in nanotube suspensions. *Appl Phys Lett*. 2001;79:2252–2254.
7. Eastman J, Choi SUS, Li S, Yu W, Thompson LJ. Anomalously increased effective thermal conductivities of ethylene-glycol-based nanofluids containing copper nanoparticles. *Appl Phys Lett*. 2001; 78(6):718–720.
8. Eastman JA, Phillpot SR, Choi SUS, Keblinski P. Thermal transport in nanofluids. *Annu Rev Mater Res*. 2004;34:219–246.
9. Keblinski P, Eastman JA, Cahill DG. Nanofluids for thermal transport. *Mater Today*. 2005;8(6):36–44.
10. Xuan Y, Li Q, Hu W. Aggregation structure and thermal conductivity of nanofluids. *AIChE J*. 2003;49(4):1038–1043.
11. Warrier P, Yuan Y, Beck MP, Teja AS. Heat transfer in nanoparticle suspensions: modeling the thermal conductivity of nanofluids. *AIChE J*. 2010;56(12):3243–3256.
12. Hanus LH, Hartzler RU, Wagner NJ. Electrolyte-induced aggregation of acrylic latex. 1. Dilute particle concentrations. *Langmuir*. 2001;17(11):3136–3147.
13. McDonogh RM, Fell CJD, Fane AG. Surface charge and permeability in the ultrafiltration of non-flocculating colloids. *J Membr Sci*. 1984;21:285–294.
14. Mondain-Mondain O, Leal-Calderon F, Phillip J, Bibette J. Depletion forces in th presence of electrostatic double layer repulsion. *Phys Rev Lett*. 1995;75(18):3364–3367.
15. Russ C, von Grunberg HH, Dijkstra M, van Roij R. Three-body forces between charged colloidal particles. *Phys Rev E*. 2002;66: 011402.
16. Tohver V, Smay JE, Braem A, Braun PV, Lewis JA. Nanoparticle halos: A new colloid stabilization mechanism. *Proc Natl Acad Sci USA*. 2001;98(16):8950–8954.
17. Uchikawa H, Hanehara S, Sawaki D. The role of steric repulsive force in the dispersion of cement particles in fresh paster prepared with organic admixture. *Cem Concr Res*. 1997;27(1):37–50.
18. Hunter RJ. *Foundations of Colloid Science*, Vol. 1. Oxford: Clarendon Press, 1987.
19. Schenkel JH, Kitchener JA. A test of the Derjaguin-Verwey-Overbeek theory with a colloidal suspension. *Trans Faraday Soc*. 1960;56:161–173.
20. Derjaguin B, Landau L. Theory of the stability of strongly charged lyophobic sols and of the adhesion of strongly charged particles in solutions of electrolytes. *Acta Phys Chem URSS*. 1941;14:633–662.
21. Verwey EJW, Overbeek JTG. *Theory of the Stability of Lyophobic Colloids*. Amsterdam: Elsevier, 1948.
22. von Smoluchowski MV. Mathematical theory of the kinetics of the coagulation of colloidal solutions. *Z Phys Chem*. 1917;92:129–168.

23. Celada AT, Salcido A. A mean field model for brownian and turbulent coagulation of polydispersed aerosols. *Rev Mexicana Fisica*. 2005;51(4):379–386.
24. Feke DL, Schowalter WR. The influence of Brownian diffusion on binary flow-induced collision rates in colloidal dispersions. *J Colloid Interface Sci*. 1985;106(1):203–214.
25. Wilhelm P, Stephan D. On-line tracking of the coating of nanoscaled silica with titania nanoparticles via zeta-potential measurements. *J Colloid Interface Sci*. 2006;293:88–92.
26. Madras G, McCoy BJ. Reversible crystal growth–dissolution and aggregation–breakage: numerical and moment solutions for population balance equations. *Powder Technol*. 2004;143–144:297–307.
27. McCoy BJ. A population balance framework for nucleation, growth, and aggregation. *Chem Eng Sci*. 2002;57(12):2279–2285.
28. McCoy BJ, Madras G. Evolution to similarity solutions for fragmentation and aggregation. *J Colloid Interface Sci*. 1998;201(2):200–209.
29. Smit DJ, Hounslow MJ, Paterson WR. Aggregation and gelation–I. Analytical solutions for CST and batch operation. *Chem Eng Sci*. 1994;49(7):1025–1035.
30. Narni NR, Peglow M, Warnecke G, Kumar J, Heinrich S, Kuipers JAM. Modeling of aggregation kernels for fluidized beds using discrete particle model simulations. *Particuology*. 2014;13:134–144.
31. Caruso F. *Colloids and Colloid Assemblies*. Weinheim: Wiley-VCH, 2004.
32. Caruso F, Fiedler H, Haage K. Assembly of [beta]-glucosidase multilayers on spherical colloidal particles and their use as active catalysts. *Colloids Surf A: Physicochem Eng Asp*. 2000;169(1–3):287–293.
33. Chen C-W, Serizawa T, Akashi M. Preparation of Platinum Colloids on Polystyrene Nanospheres and Their Catalytic Properties in Hydrogenationâ. *Chem Mater*. 1999;11(5):1381–1389.
34. Davies R, Schurr GA, Meenan P, Nelson RD, Bergna HE, Brevett CAS, Goldbaum RH. Engineered particle surfaces. *Adv Mater*. 1998;10(15):1264–1270.
35. Matijevic E. Internally and externally composite monodispersed colloidal particles. In: Pelizzetti E, editor. *Fine Particles Science and Technology: From Micro to Nanoparticles*. Dordrecht, Boston, London: Kluwer Academic Publishers, 1996:1–12.
36. Rogach A, Susha A, Caruso F, Sukhorukov G, Kornowski A, Kershaw S, Möhwald H, Eychmüller A, Weller H. Nano- and microengineering: 3-D colloidal photonic crystals prepared from sub-μm-sized polystyrene latex spheres pre-coated with luminescent polyelectrolyte/nanocrystal shells. *Adv Mater*. 2000;12(5):333–337.
37. Behrens SH, Borkovec M, Schurtenberger P. Aggregation in charge-stabilized colloidal suspensions revisited. *Langmuir*. 1998;14:1951–1954.
38. Behrens SH, Christl DI, Emmerzael R, Schurtenberger P, Borkovec M. Charging and aggregation properties of carboxyl latex particles: experiments versus DLVO theory. *Langmuir*. 2000;16(6):2566–2575.
39. Hidalgo-Alvarez R, Martin A, Fernandez A, Bastos D, Martínez F, de las Nieves FJ. Electrokinetic properties, colloidal stability and aggregation kinetics of polymer colloids. *Adv Colloid Interface Sci*. 1996;67:1–118.
40. Holthoff H, Egelhaaf SU, Borkovec M, Schurtenberger P, Sticher H. Coagulation rate measurements of colloidal particles by simultaneous static and dynamic light scattering. *Langmuir*. 1996;12(23):5541–5549.
41. Kyriakidis AS, Yiantsios SG, Karabelas AJ. A study of colloidal particle brownian aggregation by light scattering techniques. *J Colloid Interface Sci*. 1997;195(2):299–306.
42. Lin MY, Lindsay HM, Weitz DA, Ball RC, Klein R, Meakin P. Universality in colloid aggregation. *Nature*. 1989;339:360–362.
43. Lin MY, Lindsay HM, Weitz DA, Ball RC, Klein R, Meakin P. Universal reaction-limited colloid aggregation. *Phys Rev A*. 1990;41:2005–2020.
44. Kim AS, Stolzenbach KD. Aggregate formation and collision efficiency in differential settling. *J Colloid Interface Sci*. 2004;271:110–119.
45. Saltiel C, Chen Q, Manickavasagam S, Schadler LS, Siegel RW, Menguc MP. Identification of the dispersion behavior of surface treated nanoscale powders. *J Nanoparticle Res*. 2004;6(1):35–46.
46. Keblinski P, Phillpot SR, Choi SUS, Eastman JA. Mechanisms of heat flow in suspensions of nano-sized particles (nanofluids). *Int J Heat Mass Transfer*. 2002;45(4):855–863.
47. Prasher R, Phelan PE, Bhattacharya P. Effect of aggregation kinetics on the thermal conductivity of nanoscale colloidal solutions (nanofluid). *Nano Lett*. 2006;6(7):1529–1534.
48. Kretzschmar R, Holthoff H, Sticher H. Influence of pH and humic acid on coagulation kinetics of Kaolinite: a dynamic scattering study. *J Colloid Interface Sci*. 1998;202:95–103.
49. Lee D, Kim J-W, Kim BG. A New Parameter to control heat transport in nanofluids: surface charge state of the particle in suspension. *J Phys Chem B*. 2006;110:4323–4328.
50. Hemker DJ, Frank CW. Dynamic light-scattering studies of the fractal aggregation of poly(methacrylic acid) and poly(ethylene glycol). *Macromolecules*. 1990;23(20):4404–4410.
51. Kim AY, Berg JC. Fractal aggregation: scaling of fractal dimension with stability ratio. *Langmuir*. 1999;16(5):2101–2104.
52. Niklasson GA. Fractal structure of metal particle aggregates and porous materials. *Phys Scr*. 1993;1993(T49B):659–662.
53. Meakin P. Aggregation kinetics. *Phys Scr*. 1992;46(4):295–331.
54. Burns JL, Yan Y-d, Jameson GJ, Biggs S. A light scattering study of the fractal aggregation behavior of a model colloidal system. *Langmuir*. 1997;13(24):6413–6420.
55. Kruyt HR, De Jong HG. Kapillarelektrische Erscheinungen an lyophilen Solen. *Z Physik Chem*. 1922;100:250–265.
56. Derjaguin B. On the repulsive forces between charged colloid particles and on the theory of slow coagulation and stability of lyophobe sols. *Trans Faraday Soc*. 1940;35:203–215.
57. van Oss CJ. Interaction forces between biological and other polar entities in water: how many different primary forces are there? *J Dispersion Sci Technol*. 1991;12:201–219.
58. van Oss CJ. *Interfacial Forces in Aqueous Media*. New York: Marcel Dekker, 1994.
59. Hartley PG, Larson I, Scales PJ. Electrokinetic and direct force measurements between silica and mica surfaces in dilute electrolyte solutions. *Langmuir*. 1997;13:2207–2274.
60. Israelachvili J. Direct measurements of forces between surfaces in liquids at the molecular level. *Proc Natl Acad Sci USA*. 1987;84:4722–4724.
61. Israelachvilli JN, Adams GE. Direct measurement of long range forces between two mica surfaces in aqueous KNO3 solutions. *Nature*. 1976;262:774–776.
62. Le Neveu DM, Rand RP, Parsegian VA. Measurement of forces between lecithin bilayers. *Nature*. 1976;259:601–603.
63. Marcelja S, Radic N. Repulsion of interfaces due to boundary water. *Chem Phys Lett*. 1976;42(1):129–130.
64. Ninham BW. Long-range vs. short-range forces. the present state of play. *J Phys Chem*. 1980;84(12):1423–1430.
65. Prevost M, Gallez D. The role of repulsive hydration forces on the stability of aqueous black films. Application to vesicle fusion. *J Chem Soc, Faraday Trans 2: Mol Chem Phys*. 1984;80(5):517–533.
66. Snook IK, van Megen W. The solvation force between colloidal particles. *Phys Lett*. 1979;74A(5):332–334.
67. Mondain-Monval O, Leal-Calderon F, Phillip J, Bibette J. Depletion forces in the presence of electrostatic double layer repulsion. *Phys Rev Lett*. 1995;75(18):3364.
68. Fazelabdolabadi B, Walz JY, van Tassel PR. Influence of charged nanoparticles on colloidal forces: a molecular simulation study. *J Phys Chem B*. 2009;113:13860.
69. Pashley RM. DLVO and hydration forces between mica surfaces in Li+, Na+, K+, and Cs+ electrolyte solutions: a correlation of double-layer and hydration forces with surface cation exchange properties. *J Colloid Interface Sci*. 1981;83(2):531–546.
70. Molina-Bolívar JA, Ortega-Vinuesa JL. How proteins stabilize colloidal particles by means of hydration forces. *Langmuir*. 1999;15(8):2644–2653.
71. Israelachvili JN. *Intermolecular and Surface Forces, 2nd ed*. New York: Academic Press, 1992.
72. Pashley RM. Hydration forces between mica surfaces in aqueous electrolyte solutions. *J Colloid Interface Sci*. 1981;80(1):153–162.
73. Grasso D, Subramaniam K, Butkus M, Strevett K, Bergendahl J. A review of non-DLVO interactions in environmental colloidal systems. *Rev Environ Sci Biotechnol*. 2002;1(1):17–38.
74. Ise N, Sogami IS. *Structure Formation in Solution: Ionic Polymers and Colloidal Particles*. New York: Springer, 2005.
75. Fichthorn KA, Qin Y. Molecular-dynamics simulation of colloidal nanoparticle forces. *Ind Eng Chem Res*. 2006;45:5477–5481.
76. Fichthorn KA, Qin Y. Molecular dynamics simulation of the forces between colloidal nanoparticles in Lennard–Jones and n-decane solvent. *Granular Matter*. 2008;10:105–111.
77. Qin Y, Fichthorn KA. Molecular dynamics simulation of the forces between colloidal nanoparticles in n-decane solvent. *J Chem Phys*. 2007;127:144911.

78. Fazelabdolabadi B, Walz JY, van Tassel PR. Influence of charged nanoparticles on colloidal forces: a molecular simulation study. *J Phys Chem B*. 2009;113:13860–13865.
79. Peula JM, Santos R, Forcada J, Hidalgo-Alvarez R, de las Nieves FJ. Study on the colloidal stability mechanisms of acetal-functionalized latexes. *Langmuir*. 1998;14(22):6377–6384.
80. Liu L. Kinetic theory of aggregation in granular flow. *AIChE J*. 2011;57(12):3331–3343.
81. Hounslow MJ, Ryall RL, Marshall VR. A discretiszed poulation balance for nucleation, growth and aggregation. *AIChE J*. 1988;34(11): 1821–1832.
82. Hulburt HM, Katz S. Some problems in particle technology. A statistical mechanical formulation. *Chem Eng Sci*. 1964;19:555–574.
83. Randolph AD, Larson MA, editors. *Theory of Particulate Processes*. New York: Academic Press, 1971.
84. Maxwell JC. Illustrations of the dynamical theory of gases. II. On the process of diffusion of two or more kinds of moving particles among one another. *Philos Mag*. 1860;20(4):21–37.
85. Lyklema J. *Interface and Colloid Science: Soft Colloids*. London: Academic Press, 2005.
86. Hiemenz PC. *Principles of Colloid and Surface Chemistry*. New York, Basel: Marcel Dekker, Inc., 1986.
87. Corbett J, McNeill Watson F, McKnight D. An in-process instrument for the measurement of nano particle size distribution and electrophoretic mobility. PSA2008. Stratford, UK, 2008.
88. Wang XZ, Liu L, Li RF, Tweedie RJ, Primrose K, Corbett J, McNeil-Watson FK. Online characterisation of nanoparticle suspensions using dynamic light scattering, ultrasound spectroscopy and process tomography. *Chem Eng Res Des*. 2009;87(6):874–884.
89. Israelachvili JN, Pashley RM. Molecular layering of water at surfaces and origin of repulsive hydration forces. *Nature*. 1983; 306(5940):249–250.
90. Rand RP. Interacting phospholipid bilayers: measured forces and induced structural changes. *Annu Rev Biophys Bioeng*. 1981;10(1): 277–314.
91. Dukhin AS, Goetz PJ. *Ultrasound for Characterizing Colloids. Particle Sizing, Zeta Potential, Rheology*. Amsterdam, New York,Tokyo: Elsevier, 2002.
92. Chapman S, Cowling TG, editors. *The Mathematical Theory of Non-Uniform Gases*, 3rd ed. Cambridge: Cambridge University Press, 1970.
93. Pertsin A, Grunze M. Temperature dependence of the short-range repulsion between hydrated phospholipid membranes: a computer simulation study. *Biointerphases*. 2007;2(3):105–108.
94. Simon SA, Advani S, McIntosh TJ. Temperature dependence of the repulsive pressure between phosphatidylcholine bilayers. *Biophys J*. 1995;69(4):1473–1483.

Manuscript received June 20, 2014, and revision received Feb. 15, 2015.